Sitagliptin alters bone composition in high fat fed mice

Sity Aishah Mansur[1,2], Aleksandra Mieczkowska[3], Peter R Flatt[1], Daniel Chappard[3,4,5], Nigel Irwin[1], Guillaume Mabilleau[3,4,5]

[1] School of Biomedical Sciences, University of Ulster, Coleraine, Northern Ireland, United Kingdom

[2] Present address: University Tun Hussein Onn Malaysia, Johor, Malaysia

[3] GEROM Groupe Etudes Remodelage Osseux et biomatériaux – LHEA, IRIS-IBS Institut de Biologie en Santé, CHU d'Angers, LUNAM Université, 49933 ANGERS Cedex -France

[4] SCIAM, Service Commun d'Imagerie et Analyses Microscopiques, IRIS-IBS Institut de Biologie en Santé, CHU d'Angers, LUNAM Université, 49933 ANGERS Cedex – France

[5] Bone pathology unit, Angers University hospital, 49933 Angers Cedex, France

Please send all correspondence to:

Guillaume Mabilleau, PhD
GEROM-LHEA UPRES EA 4658
Institut de Biologie en Santé
Université d'Angers
4 rue larrey
49933 Angers Cedex 09
France

☎ : +33(0) 244 688 450
Fax : +33(0) 244 688 451
✉ : guillaume.mabilleau@univ-angers.fr

Short running title: Sitagliptin and bone composition

DISCLOSURE

Sity Aishah Mansur, Aleksandra Mieczkowska, Peter R Flatt, Daniel Chappard, Nigel Irwin and Guillaume Mabilleau, declare that they have no conflict of interest

Abstract: 249 words

Manuscript word count: 3,688 words

Number of figures: 2

Number of tables: 5

Number of references: 47

SUMMARY

Type 2 diabetes mellitus is associated with higher fracture risk. The present study investigated the beneficial role of sitagliptin on bone strength and bone composition in a mouse model of type 2 diabetes. Sitagliptin significantly increased bone strength by improving compromised bone composition.

ABSTRACT

Purpose/Introduction: Type 2 diabetes mellitus (T2DM) is recognized as a significant risk factor for fragility of bone. Among the newer anti-diabetic agents, dipeptidyl peptidase-4 inhibitors (DPP4i) have been reported to decrease the occurrence of bone fractures although the reason is unclear. The main aim of this study was to evaluate the impact of sitagliptin treatment on tissue bone strength and compositional parameters in the high fat fed mouse model.

Methods: Male NIH swiss mice were allowed free access to high fat diet (HFD) for 150 days to induce chronic hyperglycemia and insulin resistance. Sitagliptin was administered once daily for 3 weeks. High fat fed mice administered with saline were used as controls. Bone strength was assessed at the organ and tissue level by 3-point bending and nanoindentation, respectively. Bone microarchitecture was investigated by microcomputed tomography and bone composition was evaluated by Fourier transform infrared imaging and quantitative backscattered electron imaging.

Results: Administration of sitagliptin increased non-fasting insulin, improved glucose tolerance and increased insulin sensitivity. This was associated with clear ameliorations in bone strength at the organ and tissue level. No changes in trabecular or cortical microarchitectures were observed. On the other hand, higher values of Ca_{mean}, Ca_{turn}, collagen maturity, mineral/matrix ratio, mineral maturity and crystal size index were evidenced after sitagliptin treatment. Correlation analysis significantly linked the modifications of bone strength to changes in bone compositional parameters.

Conclusions: These results bring new light on the mode of action of sitagliptin on bone physiology and demonstrate a benefit of DPP4i.

Keywords: sitagliptin, bone fragility, bone composition, type 2 diabetes

1. INTRODUCTION

Type 1 diabetes mellitus (T1DM) and type 2 diabetes mellitus (T2DM), are associated with increased bone fragility fractures [1]. Whilst bone mineral density measurements may validate this detrimental bone effect in T1DM, this is not the case in T2DM, even after body mass index normalization [2, 3]. Although bone strength and fracture risk are assessed by measuring bone mineral density, the mechanical properties of bone are in fact determined not only by bone mass, but also by (1) the rate of bone turnover, (2) microdamage accumulation, (3) geometry/architecture of the bone, and (4) bone composition [4]. Alterations of bone turnover, microdamage accumulation and microarchitecture of bone have been studied and documented previously in T2DM [5-8]. However, although recent evidences pointed out to possible modifications of bone composition [9], data are scarce about which of these properties, i.e. post-translational collagen modifications, mineral density, mineral maturity, hydroxyapatite crystal size, ionic substitutions, etc…, are altered in T2DM.

Furthermore, little is known about the impact of clinically available antidiabetic drugs on bone composition and should be investigated in order to understand better how these molecules may affect skeletal strength. Among the newer anti-diabetic agents, dipeptidyl peptidase-4 inhibitors (DPP4i) are administered orally and exhibit HbA1c lowering effects ranged between 0.6-1.4% [10]. DPP4 has a wide variety of substrates, which have important roles in metabolism, inflammation, cell migration and differentiation. One of the important groups is represented by glucagon-like peptide-1 and -2 (GLP-1 and GLP-2, respectively), and glucose-dependent insulinotropic polypeptide (GIP). As such, the use of DPP4i prolongs action of these molecules by increasing their biological half-lives in the circulation.

Previous human studies pointed to beneficial or neutral effects of DPP4i in reducing bone fractures [11-18]. However, these studies were associated with several limitations that may hamper interpretation. Examination of skeletal response to DPP4i in preclinical diabetic animal models revealed positive effects in resisting bone fracture, despite the absence or only modest ameliorations in bone mineral density and/or trabecular and cortical bone microarchitectures [19-23], suggesting that the mechanisms behind better bone strength rely probably elsewhere than changes in bone mass or microarchitecture. With respect to the observed beneficial actions of GLP-1 and GIP on bone matrix at the tissue level [24, 25], a possible explanation could lie in amelioration of bone compositional parameters rather than bone microstructure. Therefore, the aim of the present study was to evaluate whether the DPP4i, sitagliptin, improves skeletal health in the diabetic high fat fed mice. As such, we investigated bone strength at both

the organ and tissue levels, as well as trabecular and cortical bone microarchitectures and bone compositional parameters in the NIH Swiss mice.

2. MATERIAL AND METHODS

2.1 Animals

All procedures were conducted according to UK Home Office Regulations (UK Animals Scientific Procedures Act 1986). Animal study is reported in compliance with the ARRIVE guidelines. Male NIH Swiss mice (NIH/OlaHsd) were obtained from Envigo Ltd (Blackthorn, UK) at 8 weeks of age. Animals were individually housed in an air-conditioned room at 22 ± 2°C with a 12-hour light/dark cycle, and were provided with tap water and high fat diet (HFD, 45% fat, 20% protein, 35% carbohydrate for a total of 26.2 kJ/g; Special Diet Service, Essex, UK) *ad libitum* for 150 days prior to the start of the study. At the end of the 150 days period, all mice displayed fasted blood glucose level > 14 mmol/l and higher body weight (58 ± 5 vs 47 ± 7 g, $p<0.05$) than age-matched control mice on normal laboratory chow. HFD mice were divided in two groups (n=8/group) that received once daily orally either saline (0.9% NaCl – HFD+saline) or sitagliptin phosphate monohydrate (50 mg/kg bw; ApexBio Technology, Houston, TX, USA; >97% purity – HFD+Sitagliptin) for 3 weeks at the same time of day (9 am). No adverse effects were observed following drug treatment. Eight control mice fed a normal laboratory chow (10% fat, 30% protein and 60% carbohydrate for a total of 13 kJ/g; Trouw Nutrition, Northwich, UK) and receiving once daily orally saline were used as controls.

Energy intake, body weight, plasma insulin, glucose tolerance (18 mmol/kg bw, ip, 18h fast) and insulin sensitivity (25 U/kg bw, ip) were assessed. Homeostatic model assessment of insulin resistance (HOMA-IR) and homeostatic model assessment of β-cell function (HOMA-β) were carried out using the following calculations: HOMA-IR = (fasting glucose x fasting insulin)/22.5, and HOMA-β = (20 x fasting insulin)/(fasting glucose – 3.5).

Bone mineral density (BMD, g/cm^2) and fat mass were measured with a Lunar PIXImus scanner (Inside Outside Sales, Wisconsin, U.S.A.). At necropsy, femurs and tibias were cleaned of soft tissues and stored in 70% ethanol at 4°C until used.

2.2. MicroCT

MicroCT analyses were performed on tibias with a Skyscan 1172 microtomograph (Bruker MicroCT, Kontich, Belgium) operated at 70 kV, 100 µA, 340-ms integration time. The isotropic pixel size was fixed at 4 µm, the rotation step at 0.25° and exposure was done with a 0.5-mm aluminum filter. Each 3D reconstruction image dataset was binarized using global thresholding. Trabecular volume of interest (VOI) was located 0.5 mm below the growth plate and extended on 2-mm. Cortical volume of interest extended on 1-mm centered at the midshaft tibia. All histomorphometrical parameters were determined according to guidelines and nomenclature proposed by the American Society for Bone and Mineral Research [26].

2.3. Bone histomorphometry

After microCT, tibias were embedded, undecalcified in methylmethacrylate at 4°C to preserve enzyme activities. Sagittal sections (7-µm thickness) were performed on a heavy-duty microtome equipped with a 50° tungsten carbide knife. Four non-serial sections were stained with toluidine blue for the measurement of the number of osteoblasts and adipocytes. Four additional sections were stained for the osteoclastic tartrate resistant acid phosphatase (TRAcP). Four non-consecutive sections were stained with Goldner trichrome to assess the extent of osteoid formation. Histomorphometrical parameters were determined in the proximal tibia metaphysis. Standard bone histomorphometrical nomenclatures, symbol and units were used as described in the report of the American Society for Bone and Mineral Research [27].

2.4. Bone strength assessment

Three-point bending experiments were performed on femurs after rehydrating bones at 4°C for 24 h. Femurs were loaded to failure in 3-point bending at 1 mm/min using an Instron 5942 (Instron, Elancourt, France). The lower span length was set to 10 mm. Femurs were oriented so the anterior quadrant was facing down and subjected to tensile loads. Load and displacement were digitally recorded at a sampling rate of 100 Hz and measured using a 500 N load cell (Instron). The load-displacement curve was computed with the Bluehill 3 software (Instron) and the maximum load, yield load (0.2% offset method), stiffness, post-yield displacement and work to failure were computerized. After three-point bending experiments, femurs were embedded undecalcified in polymethylmethacrylate (pMMA) at 4°C and cross-sections were made at the midshaft using a diamond saw (Accutom, Struers, Champigny sur

Marne, France). Blocks were sectioned with heavy-duty microtome equipped with a 50° tungsten carbide knife for FTIRI analyses. Samples were then polished to a 1-µm finish with diamond particles (Struers, France) before nanoindentation. Samples were subjected to rehydration in saline for 24 h. Twelve indentations, at distance from canals, osteocyte lacunae and/or microcracks were randomly positioned in cortical bone with a NHT-TTX system (Anton Paar, Les Ulis, France). Indentation depth was fixed at 900 nm with loading/unloading speed set at 40 mN/min. At maximum load, a holding period of 15 seconds was applied to avoid creeping of the bone material. The following material properties at the tissue-level, maximum load (Force max), indentation modulus (E_{IT}), indentation hardness (H_{IT}) and work of indentation (WI), corresponding to the area under the indentation curve, were determined according to Oliver and Pharr [28].

Although local mineral content influences greatly the measured parameters in nanoindentation, we did not adjust nanoindentation parameters for local mineral content because (1) the range of Ca concentration values measured by qBEI is rather narrow, making a correlation analysis difficult and uncertain, (2) there are some inherent variations in apparent calcium levels due to the counting statistics accompanying backscattered electron signal, (3) there can be variations of modulus at given mineral content due to mechanical anisotropy of the mineralized collagen matrix, (4) the only apparent formula to adjust for mineral content is dependent on aspect ratio of the mineral particles [29]. Furthermore, nanoindentation was performed before qBEI measurements and specimen were repolished with silicon carbide paper (P4000) and diamond suspension on polishing clothes before being examined under the scanning electron microscope. As such although the amount of matter removed is negligible (~6 µm), we cannot obtain a perfect match between qBEI and nanoindentation locations.

2.5. Fourier-transform infrared imaging (FTIRI)

Cross-sectional sections (4 µm) of the midshaft femur were sandwiched between barium fluoride optical windows. FTIRI was performed with a vertex 70 spectrometer (Bruker, Ettlingen, Germany) interfaced with a Hyperion 3000 microscope and a focal plane array detector (64 x 64 pixels) covering a field of view of 180 x 180 µm. Nine consecutive field-of-view were stitched together to allow sufficient bone to be analyzed. Sections were scanned with a spectral resolution of 8 cm^{-1} (spectral region 900-2000 cm^{-1}). Each spectrum was corrected for Mie scattering with the RMieS-EMSC_v5 algorithm (kind gift of Prof Peter Gardner, University of Manchester, UK) prior to be subjected to pMMA substraction. Evaluation

of spectral images was done with a lab-made routine script in Matlab R2016b (The Mathworks, Natick, MA). FTIR bone parameters [30] calculated were: (1) mineral/matrix ratio (area of υ1, υ3 phosphate/area amide1); (2) acid phosphate content (intensity ratio 1127cm^{-1}/1096 cm^{-1}); (3) mineral maturity (intensity ratio 1030 cm^{-1}/1020 cm^{-1}), reflecting crystal size and perfection; and (4) collagen maturity (intensity ratio 1660 cm^{-1}/1690 cm^{-1}). The crystal size index was introduced based on intensity ratio 1075 cm^{-1}/1055 cm^{-1}. The 1075 cm^{-1} subband has been shown to be positively and linearly correlated with crystal size in 002, 211, 200 and 202 directions determined by X-ray diffraction, whilst the 1055 cm^{-1} subband remains constant during crystal growth [31]. The carbonate/phosphate ratio (intensity υ3 carbonate located at ~1415 cm^{-1}/1030 cm^{-1}) was computed after subtracting the organic matrix spectrum [32]. Histogram distribution for each parameter were fitted with a gaussian model and considered normally distributed if the R^2 coefficient was > 0.95. In the present study, no histogram distribution deviated from normal distribution. For each of the compositional parameters, the mean and full width at half maximum of the pixel distribution (excluding the zero background values) were computed and represented as mean and heterogeneity.

2.6. Quantitative backscattered electron imaging (qBEI)

Analyses were performed on the same blocks as nanoindentation or used for FTIRI sections. Blocks were repolished to remove indentation marks at the surface of bone specimen. On average, this polishing procedure removed 6 µm of material. Blocks were carbon-coated and observed with a scanning electron microscope (EVO LS10, Carl Zeiss Ltd, Nanterre, France) equipped with a five quadrant semi-conductor backscattered electron detector. The microscope was operated at 20 keV with a probe current of 250 pA and a working distance of 15 mm. The backscattered raw signal was calibrated using pure carbon (Z=6, mean grey level = 25), pure aluminium (Z=13, mean grey level =225) and pure silicon (Z=14, mean grey level =253) standards (Micro-analysis Consultants Ltd, St Ives, UK). With this calibration, the mean grey level of pMMA resin was of 26 and the mean grey level of osteoid tissue or bone marrow was of 27. The cortical bone area was imaged at a 200X nominal magnification, corresponding to a pixel size of 0.5 µm. Two variables were obtained from the bone mineral density distribution of the full cortical shell: Ca_{mean} as the average calcium concentration and Ca_{width} as the width of the histogram at half maximum of the peak and representing calcium heterogeneity.

Furthermore, we also examined the periosteal and endosteal surfaces at a 400X nominal magnification, corresponding to a pixel size of 0.25 µm. Then, pMMA blocks were incubated with solid elemental iodine (~50 mg) for 48 hours in sealed glass jar. This staining, that allows visualization of osteoid seam in backscattered electron mode, was first proposed by Boyde and colleagues [33]. PMMA blocks were further re-examined in the SEM microscope in backscattered electron mode and periosteal and endosteal surfaces were again recorded at a X400 nominal magnification. Images of endosteal and periosteal surfaces before and after iodine staining were registered and bone packets adjacent to osteoid seam identified. On images recorded before iodine staining, a line (3 pixel width) was drawn perpendicular to the osteoid seam and extended in the mineralized bone matrix using ImageJ 1.51s. The mean grey level of each pixel of this line was computed and plotted against the distance from the mineralization front. Biphasic profile were obtained at every locations. As the mineralization process of bone is biphasic, slopes of primary and secondary mineralization as well as the Ca_{turn} value, representing the calcium concentration where the primary mineralization process changes to secondary mineralization process, were computed.

2.7 Biochemical analyses

For the determination of mineral composition, left tibias and femurs (n=4/group) were flushed of bone marrow, left to dry overnight at 60°C and weighted on a precision scale (Scaltex, SBC 32, 0.1 mg accuracy). Dry samples were ashed in a muffle furnace (Vecstar Furnace 91e, Eurotherm controls, Nantes, France) at 650°C for 18 hours and ashes were weighted on a precision scale as above. Ash weight was expressed as percentage of dry bone. Ashes were crushed in a fine powder, dissolved in 0.5 M HCl and calcium and phosphate concentrations were determined with an automated spectrophotometer as described elsewhere [34].

Left tibias and femurs (n=4/group) were powdered and demineralized with 0.5M EDTA in 0.05M Tris buffer saline for 48 hours at 4°C, reduced with 1% $NaBH_4$ at 37°C for 1 hour and hydrolyzed in 6N HCl at 110°C for 24 hours in a sealed glass tube. Cross-links were separated by high-performance liquid chromatography. Dihydrolysinonorleucine (DHLNL) was identified and detected by post-column derivatization using O-phthaldehyde whilst pyridinoline (Pyr) and pentosidine (Pen) were detected by natural fluorescence with excitation at 295 nm and 335 nm and emission at 395 nm and 385 nm, respectively. Hydroxyproline content was measured by HPLC using the hydroxyproline by HPLC Bio-

Rad kit. Collagen content was estimated from the hydroxyproline content assuming that collagen weighted 7.5 times the measured hydroxyproline weight, with a molecular weight of 300,000. The resulting data were used to calculate the cross-link content as moles per mole of collagen.

2.8. Statistical analysis

Due to the adaptive nature of bone, data were adjusted for body mass using a linear regression method as reported in detail elsewhere [35]. One-way analyses of variance with Tukey multiple comparison test were employed to test for significance between lean+saline, HFD+saline and HFD+sitaglitpin animals at the exception of ash weight, calcium and phosphate content and collagen cross-link concentrations, where a non-parametrical Kruskal-Wallis test with Dunn's multiple comparisons were performed. Stepwise multiple linear regressions using the equation:

$$\text{Bone stiffness} = f(\beta_0 + \beta_1.\text{HOMA-IR} + \beta_2.\text{Tt.Ar} + \beta_3.\text{Ct.Th} + \beta_4.\text{collagen maturity} + \beta_5.\text{mineral maturity} + \beta_6.\text{mineral/matrix ratio} + \beta_7.\text{carbonate/phosphate ratio})$$

were computerized to evaluate how bone stiffness is influenced by insulin resistance, cortical bone microarchitecture and composition. Differences at p equal to or less than 0.05 were considered significant.

3. RESULTS

3.1. Sitagliptin ameliorates metabolic parameters but not bone mineral densities

As presented in Table 1, high fat diet resulted in higher body and fat masses by 24% (p=0.003) and 37% (p=0.001), respectively. Although food intakes were similar, the higher energy content of high fat chow led to a significant increase in energy intake by 93% (p=0.001). Glucose tolerance and insulin sensitivity were also significantly impaired in HFD+saline animals as compared with lean+saline. Administration of sitagliptin in high fat fed animals resulted in higher non-fasting insulin level (55%, p=0.045), and improved glucose tolerance (32%, p=0.043), insulin sensitivity (30%, p=0.048), HOMA-IR (24%, p=0.009) and HOMA-β (42%, p=0.030) indexes.

However, bone mineral density assessed at either the whole body, or lumbar and femur sites, revealed no significant differences between the three groups of animals.

3.2. Sitagliptin ameliorates whole bone stiffness and tissue bone strength

Next, we thought to determine whether high fat diet resulted in lower bone strength. Indeed, we observed that as compared with lean+saline animals, HFD+saline mice presented with lower ultimate load (-28%, p=0.002), stiffness (-33%, p=0.001), post-yield displacement (-45%, p=0.021) and work-to-fracture (-35%, p=0.019) (Table 2). Administration of sitagliptin significantly augmented bone stiffness by 15% (p=0.019). Tissue level mechanical properties were estimated from whole-bone mechanical tests using equations from engineering beam theory. As compared with saline animals, HFD+saline mice presented with lower ultimate stress (-43%, p<0.001), yield stress (-38%, p<0.001) and elastic modulus (-48%, p<0.001). Administration of sitagliptin resulted in significant higher values of ultimate stress (24%, p=0.021), yield stress (20%, p=0.021) and elastic modulus (30%, p=0.041). Tissue level mechanical properties were also determined by nanoindentation. HFD resulted in lower maximum force (-22%, p=0.001), indentation modulus (-21%, p<0.001), indentation hardness (-27%, p=0.003) and work of indentation (-23%, p<0.001). Administration of sitagliptin increased indentation modulus by 12 % (p=0.041) in HFD animals (Table 2). Sitagliptin increased almost significantly indentation hardness (p=0.079) in HFD animals.

3.3. Sitagliptin has no effects on trabecular and cortical microarchitectures, but augments osteoid surfaces and the numbers of osteoblasts and marrow adipocytes

As bone strength at the organ level depends on bone structural and bone compositional properties, we next investigated cortical and trabecular bone microarchitectures (Table 3). As compared with lean+saline animals, HFD+saline mice presented with lower cross-sectional area, cortical area, cortical thickness, cortical bone density, trabecular bone volume and trabecular numbers. Administration of sitagliptin did not modify neither cortical nor trabecular bone microarchitectures.

Histomorphometrical analysis of proximal tibia metaphysis revealed significant decreases in osteoid perimeter in HFD animals. However, administration of sitagliptin significantly increased osteoid perimeter by 92% as compared with HFD+saline animals. No differences in osteoid thickness were encountered between the three groups of animals. At the cellular level, HFD led to significant augmentations in the number of osteoclasts and adipocytes whilst the number of osteoblasts is reduced (Table 3). After sitagliptin administration, the number of osteoclasts was significantly lower (-48%, p=0.001) whilst osteoblast and adipocyte numbers were significantly higher (32%, p=0.001 and 77%, p<0.001, respectively).

3.4. Sitagliptin modifies bone compositional parameters in HFD mice

As bone composition is suspected to be altered in T2DM, we first investigated how high fat diet may influence bone composition. Tissue mineral density within the cortical bone matrix was examined first. As represented in Figure 1A and supported by the bone mineral density distribution curves, HFD+saline animals exhibit a trend to lower calcium value. Indeed, the mean calcium concentration, Ca_{mean}, was significantly reduced by 21% ($p<0.001$) without alterations of the calcium distribution heterogeneity, Ca_{width}. To assess whether mineralization kinetic was altered, we analyzed bone mineralization profile at site of new bone formation in cortical bone (Figure 1B). Mineralization of osteoid tissue is a biphasic process characterized by a rapid primary mineralization followed by slower secondary mineralization. The calcium concentration at which primary mineralization is replaced by secondary mineralization, Ca_{turn}, was significantly reduced by 19% ($p<0.001$) in HFD+saline animals as compared with lean+saline mice and supported by lower primary mineralization slope (-14%, $p<0.001$) rather than change in secondary mineralization slope. Administration of sitagliptin in HFD animals led to slight but significant higher Ca_{mean} (5%, $p=0.009$), Ca_{turn} (10%, $p=0.042$) and slope of primary mineralization (8%, $p=0.038$). To further investigate compositional changes in the bone matrix, we examined thin bone sections by Fourier transform infrared imaging (FTIRI). Figure 2A represents FTIRI images over the cortical width of the lean+saline, HFD+saline and HFD+sitagliptin groups. Some differences in the pixel intensity distribution in the bone matrix were noted, especially for the mineral/matrix (M/M) ratio, mineral maturity (XST) and mineral crystal size index (CSI). Indeed, as compared with lean+saline animals, HFD+saline mice presented with significant lower collagen maturity (-23%, $p<0.001$), mineral maturity (-20%, $p<0.001$), crystal size index (-18%, $p<0.001$), mineral/matrix ratio (-27%, $p<0.001$) and carbonate/phosphate ratio (-19%, $p=0.01$). Administration of sitagliptin to HFD mice led to significant augmentations in collagen maturity by 12 % ($p=0.048$), mineral maturity by 4 % ($p<0.001$), crystal size index by 4% ($p<0.001$) and mineral/matrix ratio by 16% ($p=0.045$) (Figure 2B). In addition, heterogeneities of all the bone mineral or collagen parameters measured by FTIRI were not significantly different between the three groups of animals.

Next, bone mineral content and collagen cross-link profiles were determined chemically (Table 4). Ash weight, calcium and phosphate content were significantly lower in HFD+saline animals as compared with lean+saline. Furthermore, a more pronounced reduction in enzymatic mature (Pyr) vs. immature

(DHLNL) collagen cross-links was observed in these animals. Non-enzymatic collagen cross-link, indicative of advanced glycation endproducts represented by the pentosidine content, was significantly and dramatically augmented in HFD+saline animals. Administration of sitagliptin led to significant higher values of calcium and non-significant higher phosphate (p=0.078). Mature and immature enzymatic collagen cross-links were also significantly augmented whilst the pentosidine content was significantly lowered.

3.5. Changes in bone compositional parameters, cortical bone microarchitecture and insulin resistance are strong predictors of bone stiffness

In order to better understand which of the above changes in cortical bone microarchitecture, bone composition and insulin resistance were directly linked to modifications of bone stiffness, we performed multiple linear regression analysis (Table 5). Data were dichotomized by groups. When only lean+saline and HFD+saline animals were considered, the multiple regression model exhibited an adjusted R^2 value of 0.786, indicating that more than 78% variation in bone stiffness could be explain by changes in mineral/matrix ratio, cross-sectional tissue area and HOMA-IR. When HFD+saline and HFD+sitagliptin animals were considered, the multiple regression model exhibited an adjusted R^2 value of 0.696 suggesting that the model fitted strongly with the experimental data. Predictors were mineral/matrix ratio, collagen maturity and HOMA-IR.

4. DISCUSSION

Type 2 diabetes mellitus progress worldwide and has been recognized as a risk factor for bone frailty. Among the glucose-lowering agents approved for the treatment of T2DM, some of them have been associated with detrimental actions on bone itself. As such, it is of utmost importance to assess the possible actions of glucose-lowering agents on bone physiology. Although sitagliptin was the first DPP4i approved in 2006, little is known about its effects on bone composition. Previous reports highlighted positive effects in resisting bone fracture, despite the absence or only modest ameliorations in bone mineral densities and/or bone microarchitectures [19, 22, 23, 36]. Taken together, these results suggested that the mechanisms behind better bone strength rely beyond changes in the quantity of bone or its structural properties.

Although T2DM is multifactorial, the high fat-fed swiss mice employed in the present study, presented with elevated fasted blood glucose level above 14 mmol/l and insulin resistance making this model a clear type 2 diabetic animal model. In these mice, bone strength was reduced by a combination of structural (Tt.Ar, Ct.Ar, Ct.Ar/Tt.Ar, Ct.Th) and compositional (collagen maturity, collagen cross-links profile, pentosidine content, mineral/matrix ratio, mineral crystallinity, crystal size, carbonate/phosphate ratio) alterations as well as insulin resistance. Bone strength was assessed by 3-point bending, which is a simple and reproducible test to estimate bone strength. However, the relevance of such biomechanical test to the mechanisms of fragility fracture in humans is questionable.

Human data on modification of bone composition at the tissue level in diabetes mellitus are scarce and limited to mechanical effects at the microscale. Rodent model of diabetes mellitus have previously revealed alterations of bone matrix composition. In type 1 diabetes mellitus, although alteration of the mineral component of the bone matrix vary between animal models, clear alterations of the collagen moiety were evident with a reduction in enzymatic collagen cross-links and an elevation in non-enzymatic collagen cross-linking [37-39]. In T2DM, Hammond et al. investigated the bone composition in the Zucker diabetic Sprague-Dawley rat, a model of spontaneous T2DM [40]. This study highlighted that the degree of mineralization of the bone matrix, assessed by ash fraction and bone mineral density, was significantly lower in diabetic animals despite no modifications of the mineral composition, i.e. mineral crystallinity and carbonate substitution. However, alterations of collagen fibers with higher D-spacing were evident. This study also highlighted that the site of investigation (periosteal surfaces vs. whole bone) and the choice of the method of investigation (vibrational vs. physical method) could result in conflicting data. Indeed, the authors concluded that accumulation of advanced glycation endproducts in the collagen matrix may result in modification of the Raman signature of the collagen structure and hence a biased mineral/matrix ratio. In the present study, we used a combination of Fourier transform infrared spectroscopy and electron microscopy over the full cortical width, and performed biochemical analyses of whole bone. All these data pointed out to a lower degree of mineralization of the bone matrix, alterations of crystal size, lower enzymatic collagen cross-linking and higher accumulation of advanced glycation endproducts. Multiple regression analyses suggested that lower mineral/matrix ratio and cross-sectional area were strong predictors of bone stiffness whilst insulin resistance, although associated with lower bone stiffness, was less important. Nevertheless, the indirect consequences of insulin resistance on bone cells and hence deposition/modification of bone matrix cannot be neglected.

The present results support also that short-term treatment with sitagliptin was sufficient to increase bone stiffness in HFD mice. The mechanism relied on modification of bone compositional properties rather than action on structural parameters. Multiple regression analyses highlighted here again the strong influence of mineral/matrix ratio, and hence the degree of mineralization of the bone matrix, collagen maturity and to a lower extent insulin resistance.

To note is the higher number of osteoblasts and adipocytes found at the surface of bone and in the bone marrow, respectively. A recent elegant study from Ambrosi et al., demonstrated that DPP4 is expressed by adipogenic progenitor cells that block the differentiation of osteogenic progenitor cells [41]. As such, a plausible scenario to explain the higher osteoblast numbers and possibly the positive effects on bone composition may reside in the direct blockade of adipocyte-derived DPP4. This hypothesis would need to be demonstrated in the future but also to be verified in human tissues. Furthermore, some recent investigations conducted in diabetic and osteoporotic rodents (10-300 mg/kg/day sitagliptin), as well as in human postmenopausal diabetic women, suggest a reduction in bone resorption with sitagliptin [22, 36, 42] supporting the lower number of osteoclasts observed in the present study.

Another plausible scenario is represented by changes in the deposition of non-collagenous protein involved in the regulation of bone mineralization that could change the mineralization kinetic. This idea is further supported by the greater values of primary mineralization slope and Ca_{turn}, observed in the present study, and could indicate changes in the control of mineral deposition in the bone matrix. Greater mineralization degree in addition to higher mineral crystallinity and crystal size may also be interpreted by modifications in the control of mineral deposition in bone.

A limitation to this study is the lack of double administration of fluorochrome. We could not measure dynamic histomorphometrical indexes and we could not measure precisely by Fourier transform infrared microspectroscopy the effects of sitagliptin administration at bone forming site.

Another limitation is represented by the fact that the present study was conducted in a rodent model of type 2 diabetes mellitus and not in humans. Bone biopsies of human individuals suffering of type 2 diabetes mellitus are rare worldwide. The amount of specimen is even lower if only DPP4i-treated patients are considered. As such, due to species differences at all levels, it is difficult to guarantee that the observed beneficial role of sitagliptin in our rodent model may be extrapolated to humans.

In conclusion, the present study provides new insight in to the mode of action of sitagliptin on bone in diabetes. Indeed, sitagliptin ameliorated bone biomechanical properties by positively modifying bone composition rather than affecting bone microstructure. Further studies are required to ascertain whether such effects occur in humans, but the results of this study are highly encouraging to the goal of improving bone strength in type-2 diabetes and aiding clinicians regarding selection of anti-diabetic drugs in patients at high risk of bone fractures.

5. ACKNOWLEDGEMENTS

The authors are grateful to Nadine Gaborit and Stéphanie Lemière (University of Angers, GEROM-LHEA, Institut de Biologie en Santé, Angers, France) for their help with microCT. This work was supported by grants from the Irish Endocrine Society as well as University of Ulster Research Challenge Fund and Proof of Principle Funding Programs.

6. REFERENCES

1. Janghorbani M, Van Dam RM, Willett WC, Hu FB (2007) Systematic review of type 1 and type 2 diabetes mellitus and risk of fracture. Am J Epidemiol 166:495-505
2. Strotmeyer ES, Cauley JA, Schwartz AV, Nevitt MC, Resnick HE, Zmuda JM, Bauer DC, Tylavsky FA, de Rekeneire N, Harris TB, Newman AB, Health ABCS (2004) Diabetes is associated independently of body composition with BMD and bone volume in older white and black men and women: The Health, Aging, and Body Composition Study. J Bone Miner Res 19:1084-1091
3. Vestergaard P (2007) Discrepancies in bone mineral density and fracture risk in patients with type 1 and type 2 diabetes--a meta-analysis. Osteoporos Int 18:427-444
4. Burr DB (2004) Bone quality: understanding what matters. J Musculoskelet Neuronal Interact 4:184-186
5. Burghardt AJ, Issever AS, Schwartz AV, Davis KA, Masharani U, Majumdar S, Link TM (2010) High-resolution peripheral quantitative computed tomographic imaging of cortical and trabecular bone microarchitecture in patients with type 2 diabetes mellitus. J Clin Endocrinol Metab 95:5045-5055
6. Krakauer JC, McKenna MJ, Buderer NF, Rao DS, Whitehouse FW, Parfitt AM (1995) Bone loss and bone turnover in diabetes. Diabetes 44:775-782
7. Patsch JM, Burghardt AJ, Yap SP, Baum T, Schwartz AV, Joseph GB, Link TM (2013) Increased cortical porosity in type 2 diabetic postmenopausal women with fragility fractures. J Bone Miner Res 28:313-324
8. Tang SY, Vashishth D (2010) Non-enzymatic glycation alters microdamage formation in human cancellous bone. Bone 46:148-154
9. Farr JN, Drake MT, Amin S, Melton LJ, 3rd, McCready LK, Khosla S (2014) In vivo assessment of bone quality in postmenopausal women with type 2 diabetes. J Bone Miner Res 29:787-795
10. Dicker D (2011) DPP-4 inhibitors: impact on glycemic control and cardiovascular risk factors. Diabetes Care 34 Suppl 2:S276-278
11. Choi HJ, Park C, Lee YK, Ha YC, Jang S, Shin CS (2016) Risk of fractures and diabetes medications: a nationwide cohort study. Osteoporos Int 27:2709-2715

12. Dombrowski S, Kostev K, Jacob L (2017) Use of dipeptidyl peptidase-4 inhibitors and risk of bone fracture in patients with type 2 diabetes in Germany-A retrospective analysis of real-world data. Osteoporos Int 28:2421-2428
13. Driessen JH, van den Bergh JP, van Onzenoort HA, Henry RM, Leufkens HG, de Vries F (2017) Long-term use of dipeptidyl peptidase-4 inhibitors and risk of fracture: A retrospective population-based cohort study. Diabetes Obes Metab 19:421-428
14. Josse RG, Majumdar SR, Zheng Y, Adler A, Bethel MA, Buse JB, Green JB, Kaufman KD, Rodbard HW, Tankova T, Westerhout CM, Peterson ED, Holman RR, Armstrong PW, Group TS (2017) Sitagliptin and risk of fractures in type 2 diabetes: Results from the TECOS trial. Diabetes Obes Metab 19:78-86
15. Mamza J, Marlin C, Wang C, Chokkalingam K, Idris I (2016) DPP-4 inhibitor therapy and bone fractures in people with Type 2 diabetes - A systematic review and meta-analysis. Diabetes Res Clin Pract 116:288-298
16. Monami M, Dicembrini I, Antenore A, Mannucci E (2011) Dipeptidyl peptidase-4 inhibitors and bone fractures: a meta-analysis of randomized clinical trials. Diabetes Care 34:2474-2476
17. Mosenzon O, Wei C, Davidson J, Scirica BM, Yanuv I, Rozenberg A, Hirshberg B, Cahn A, Stahre C, Strojek K, Bhatt DL, Raz I (2015) Incidence of Fractures in Patients With Type 2 Diabetes in the SAVOR-TIMI 53 Trial. Diabetes Care 38:2142-2150
18. Yang J, Huang C, Wu S, Xu Y, Cai T, Chai S, Yang Z, Sun F, Zhan S (2017) The effects of dipeptidyl peptidase-4 inhibitors on bone fracture among patients with type 2 diabetes mellitus: A network meta-analysis of randomized controlled trials. PLoS One 12:e0187537
19. Cusick T, Mu J, Pennypacker BL, Li Z, Scott KR, Shen X, Fisher JE, Langdon RB, Kimmel DB, Zhang BB, Glantschnig H (2013) Bone loss in the oestrogen-depleted rat is not exacerbated by sitagliptin, either alone or in combination with a thiazolidinedione. Diabetes Obes Metab 15:954-957
20. Eom YS, Gwon AR, Kwak KM, Kim JY, Yu SH, Lee S, Kim YS, Park IB, Kim KW, Lee K, Kim BJ (2016) Protective Effects of Vildagliptin against Pioglitazone-Induced Bone Loss in Type 2 Diabetic Rats. PLoS One 11:e0168569
21. Gallagher EJ, Sun H, Kornhauser C, Tobin-Hess A, Epstein S, Yakar S, LeRoith D (2014) The effect of dipeptidyl peptidase-IV inhibition on bone in a mouse model of type 2 diabetes. Diabetes Metab Res Rev 30:191-200
22. Glorie L, Behets GJ, Baerts L, De Meester I, D'Haese PC, Verhulst A (2014) DPP IV inhibitor treatment attenuates bone loss and improves mechanical bone strength in male diabetic rats. Am J Physiol Endocrinol Metab 307:E447-455
23. Kyle KA, Willett TL, Baggio LL, Drucker DJ, Grynpas MD (2011) Differential effects of PPAR-{gamma} activation versus chemical or genetic reduction of DPP-4 activity on bone quality in mice. Endocrinology 152:457-467
24. Mabilleau G, Mieczkowska A, Irwin N, Flatt PR, Chappard D (2013) Optimal bone mechanical and material properties require a functional glucagon-like peptide-1 receptor. J Endocrinol 219:59-68
25. Mieczkowska A, Irwin N, Flatt PR, Chappard D, Mabilleau G (2013) Glucose-dependent insulinotropic polypeptide (GIP) receptor deletion leads to reduced bone strength and quality. Bone 56:337-342
26. Bouxsein ML, Boyd SK, Christiansen BA, Guldberg RE, Jepsen KJ, Muller R (2010) Guidelines for assessment of bone microstructure in rodents using micro-computed tomography. J Bone Miner Res 25:1468-1486
27. Parfitt AM, Drezner MK, Glorieux FH, Kanis JA, Malluche H, Meunier PJ, Ott SM, Recker RR (1987) Bone histomorphometry: standardization of nomenclature, symbols, and units. Report of the ASBMR Histomorphometry Nomenclature Committee. J Bone Miner Res 2:595-610
28. Oliver WC, Pharr GM (1992) An improved technique for determining hardness and elastic modulus using load and displacement sensing indentation experiments. J Mater Res 7:1564-1583

29. Gupta HS, Schratter S, Tesch W, Roschger P, Berzlanovich A, Schoeberl T, Klaushofer K, Fratzl P (2005) Two different correlations between nanoindentation modulus and mineral content in the bone-cartilage interface. J Struct Biol 149:138-148
30. Paschalis EP (2012) Fourier transform infrared imaging of bone. Methods Mol Biol 816:517-525
31. Gadaleta SJ, Paschalis EP, Betts F, Mendelsohn R, Boskey AL (1996) Fourier transform infrared spectroscopy of the solution-mediated conversion of amorphous calcium phosphate to hydroxyapatite: new correlations between X-ray diffraction and infrared data. Calcif Tissue Int 58:9-16
32. Ou-Yang H, Paschalis EP, Mayo WE, Boskey AL, Mendelsohn R (2001) Infrared microscopic imaging of bone: spatial distribution of CO3(2-). J Bone Miner Res 16:893-900
33. Boyde A, McCorkell FA, Taylor GK, Bomphrey RJ, Doube M (2014) Iodine vapor staining for atomic number contrast in backscattered electron and X-ray imaging. Microsc Res Tech 77:1044-1051
34. Mabilleau G, Filmon R, Petrov PK, Basle MF, Sabokbar A, Chappard D (2010) Cobalt, chromium and nickel affect hydroxyapatite crystal growth in vitro. Acta Biomater 6:1555-1560
35. Jepsen KJ, Silva MJ, Vashishth D, Guo XE, van der Meulen MC (2015) Establishing biomechanical mechanisms in mouse models: practical guidelines for systematically evaluating phenotypic changes in the diaphyses of long bones. J Bone Miner Res 30:951-966
36. Wang C, Xiao F, Qu X, Zhai Z, Hu G, Chen X, Zhang X (2017) Sitagliptin, An Anti-diabetic Drug, Suppresses Estrogen Deficiency-Induced OsteoporosisIn Vivo and Inhibits RANKL-Induced Osteoclast Formation and Bone Resorption In Vitro. Front Pharmacol 8:407
37. Mansur SA, Mieczkowska A, Bouvard B, Flatt PR, Chappard D, Irwin N, Mabilleau G (2015) Stable Incretin Mimetics Counter Rapid Deterioration of Bone Quality in Type 1 Diabetes Mellitus. J Cell Physiol 230:3009-3018
38. Mieczkowska A, Mansur SA, Irwin N, Flatt PR, Chappard D, Mabilleau G (2015) Alteration of the bone tissue material properties in type 1 diabetes mellitus: A Fourier transform infrared microspectroscopy study. Bone 76:31-39
39. Rubin MR, Paschalis EP, Poundarik A, Sroga GE, McMahon DJ, Gamsjaeger S, Klaushofer K, Vashishth D (2016) Advanced Glycation Endproducts and Bone Material Properties in Type 1 Diabetic Mice. PLoS One 11:e0154700
40. Hammond MA, Gallant MA, Burr DB, Wallace JM (2014) Nanoscale changes in collagen are reflected in physical and mechanical properties of bone at the microscale in diabetic rats. Bone 60:26-32
41. Ambrosi TH, Scialdone A, Graja A, Gohlke S, Jank AM, Bocian C, Woelk L, Fan H, Logan DW, Schurmann A, Saraiva LR, Schulz TJ (2017) Adipocyte Accumulation in the Bone Marrow during Obesity and Aging Impairs Stem Cell-Based Hematopoietic and Bone Regeneration. Cell Stem Cell 20:771-784 e776
42. Hegazy SK (2015) Evaluation of the anti-osteoporotic effects of metformin and sitagliptin in postmenopausal diabetic women. J Bone Miner Metab 33:207-212

7. FIGURE LEGENDS

Figure 1 [On-line color only]: Effects of high fat diet and sitagliptin on tissue mineral distribution. Bone mineral density distribution was evaluated by qBEI in lean+saline, HFD+saline and HFD+sitagliptin. (A) Representative calcium maps with their respective calcium distribution. Ca_{mean} represents the mean degree of mineralization and Ca_{width} represents the heterogeneity in the degree of mineralization. Values are means ± SEM for 8 mice. **: p<0.01 and ***: p<0.001 vs. HFD+saline. ###: p<0.001 vs. lean+saline. (B) Bone mineralization profile. The slopes of primary and secondary mineralization have been computerized as well as Ca_{turn} that represents the calcium concentration at which primary mineralization is followed by secondary mineralization. Values are means ± SEM for 8 mice. *: p<0.05 and ***: p<0.001 vs. HFD+saline. #: p<0.05 vs. lean+saline.

Figure 2 [On-line color only]: Effects of high fat diet and sitagliptin on compositional parameters of the bone matrix. Bone composition parameters were also assessed by Fourier transform infrared imaging (FTIRI). (A) Some FTIRI images are presented. The pseudo-color represents the degree of each parameter overall the full width of the cortical bone. CCL: collagen maturity, XST: mineral maturity, CSI: crystal size index, M/M: mineral/matrix ratio, C/P: carbonate/phosphate ratio and AcP: acid phosphate content. (B) The mean and heterogeneity of each parameter was also investigated and represented next to FTIRI images. Values are means ± SEM for 8 mice. *: p<0.05, **: p<0.01 and ***: p<0.001 vs. HFD+saline. #: p<0.05, ##: p<0.01 and ###: p<0.001 vs. lean+saline.

8. TABLES

Table 1: Metabolic parameters after 3 weeks administration of saline or sitagliptin

	Lean+saline	HFD+saline	HFD+sitagliptin
Body mass (g)	45 ± 2^{aa}	56 ± 1	54 ± 1^{bb}
Fat mass (%)	25 ± 1^{aa}	34 ± 1	32 ± 1^{b}
Food intake (g/day) (kj/day)	4.2 ± 0.3	4.1 ± 0.5	3.9 ± 0.7
Energy intake (kj/day)	55 ± 4^{aa}	106 ± 12	102 ± 16^{b}
Non-fasting insulin (ng/ml)	1.7 ± 0.6	2.0 ± 0.4	3.1 ± 0.3^{a}
$AUC_{0\text{-}60min}$ Glucose tolerance (mmol/l.min)	417 ± 32^{aaa}	614 ± 40	418 ± 74^{a}
$AUC_{0\text{-}60min}$ insulin sensitivity (ng/ml.min)	97 ± 11^{a}	58 ± 10	139 ± 36^{a}
HOMA-IR	5.4 ± 0.5	6.6 ± 0.5	4.4 ± 0.5^{aa}
HOMA-β	604 ± 89	276 ± 265	1048 ± 176^{a,b}
Whole body BMD (mg/cm²)	61 ± 1	64 ± 1	64 ± 1
Lumbar BMD (mg/cm²)	60 ± 1	68 ± 1	66 ± 4
Femur BMD (mg/cm²)	105 ± 4	111 ± 2	116 ± 3

Values are means ± SEM for 8 mice. ^{a}: p<0.05, ^{aa}: p<0.01 and ^{aaa}: p<0.001 vs. HFD+saline. ^{b}: p<0.05, ^{bb}: p<0.01 and ^{bbb}: p<0.001 vs. Lean+saline.

Table 2: Whole-bone and tissue-level mechanical properties

	Lean+saline	HFD+saline	HFD+sitagliptin
Whole-bone level			
Maximum load (N)	32 ± 2^{aa}	23 ± 1	24 ± 1
Stiffness (N/mm)	159 ± 11^{aa}	106 ± 4	123 ± 4^{a}
Postyield displacement (mm)	0.28 ± 0.03^{a}	0.16 ± 0.02	0.26 ± 0.06
Work-to-fracture (N.mm)	9.3 ± 0.8^{a}	6.1 ± 0.5	7.8 ± 0.8
Tissue level (3-point bending)			
Ultimate stress (MPa)	237 ± 12^{aaa}	136 ± 4	168 ± 4$^{a, bbb}$
Yield stress (MPa)	192 ± 8^{aaa}	120 ± 3	143 ± 5$^{a, bbb}$
Elastic modulus (GPa)	11.1 ± 1.0^{aaa}	5.7 ± 0.3	7.4 ± 0.1$^{a, bb}$
Tissue level (Nanoindentation)			
Maximum force (mN)	14.3 ± 0.7^{aa}	11.2 ± 0.2	11.7 ± 0.4^{bb}
Indentation modulus (GPa)	15.7 ± 0.6^{aa}	12.3 ± 0.5	13.8 ± 0.3^{a,bb}
Indentation hardness (MPa)	786 ± 51^{aa}	577 ± 23	690 ± 26
Work of indentation (pJ)	3488 ± 116^{aaa}	2688 ± 91	2929 ± 72^{bb}

Values are means ± SEM for 8 mice. ^{a}: p<0.05, ^{aa}: p<0.01 and ^{aaa}: p<0.001 vs. HFD+saline. ^{b}: p<0.05, ^{bb}: p<0.01 and ^{bbb}: p<0.001 vs. lean+saline.

Table 3: Microarchitectural and histomorphometrical properties of cortical and trabecular bone after saline or sitagliptin administration in high fat fed mice

	Lean+saline	HFD+saline	HFD+sitagliptin
Cortical bone			
Tt.Ar (mm^2)	2.2 ± 0.1$^{\mathbf{a}}$	1.9 ± 0.1	2.0 ± 0.1
Ma.Ar (mm^2)	0.8 ± 0.0	0.7 ± 0.1	0.9 ± 0.1
Ct.Ar (mm^2)	1.4 ± 0.0$^{\mathbf{aaa}}$	1.1 ± 0.0	1.2 ± 0.0$^{\mathbf{bbb}}$
Ct.Ar/Tt.Ar (%)	74 ± 1$^{\mathbf{aaa}}$	57 ± 2	55 ± 2$^{\mathbf{bbb}}$
Ct.Th (µm)	246 ± 5$^{\mathbf{aaa}}$	191 ± 5	191 ± 6$^{\mathbf{bbb}}$
Trabecular bone			
BV/TV (%)	21.0 ± 0.7$^{\mathbf{aaa}}$	11.8 ± 0.8	10.8 ± 1.1$^{\mathbf{bbb}}$
Tb.N (1/mm)	3.1 ± 0.1$^{\mathbf{aaa}}$	1.5 ± 0.2	1.5 ± 0.2$^{\mathbf{bbb}}$
Tb.Th (µm)	77 ± 2	76 ± 5	67 ± 3
Tb.Sp (µm)	260 ± 9	295 ± 25	299 ± 20
OS/BS (%)	4.1 ± 0.5^{aaa}	1.4 ± 0.3	2.7 ± 0.4^{aa,bb}
O.Th (µm)	2.3 ± 0.5	3.4 ± 1.0	3.3 ±1.0
N.Ob/B.Pm (1/mm)	2.5 ± 0.1$^{\mathbf{aa}}$	1.8 ± 0.1	3.3 ± 0.4$^{\mathbf{aa,b}}$
N.Oc/B.Pm (1/mm)	0.6 ± 0.1$^{\mathbf{aa}}$	1.2 ± 0.2	0.6 ± 0.1$^{\mathbf{aa}}$
N.Ad/Ma.Ar (1/mm^2)	20 ± 1$^{\mathbf{aa}}$	35 ± 2	61 ± 5$^{\mathbf{aaa,bbb}}$

Values are means ± SEM for 8 mice. ^{a}: p<0.05, ^{aa}: p<0.01 and ^{aaa}: p<0.001 vs. HFD+saline. ^{bbb}: p<0.001 vs. Lean+saline.

Table 4: Bone mineral content and collagen cross-link profiles

	Lean+saline	HFD+saline	HFD+sitagliptin
Ash weight (%)	59.5 ± 1.2^{aa}	52.0 ± 0.4	55.4 ± 0.6
Calcium (mg/g ash)	362 ± 2^{aa}	339 ± 1	351 ± 1^{a}
Phosphate (mg/g ash)	194 ± 1^{aa}	184 ± 1	190 ± 1
Pyr (mmol/mol collagen)	238 ± 18^{aa}	160 ± 9	193 ± 9^{a}
DHLNL (mmol/mol collagen)	668 ± 24^{aa}	520 ± 14	583 ± 13^{a}
Pentosidine (mmol/mol collagen)	75 ± 10^{aaa}	270 ± 16	198 ± 11^{a}

Values are means ± SEM for 4 mice/group. ^{a}: p<0.05, ^{aa}: p<0.01 and ^{aaa}: p<0.001 vs. HFD+saline. ^{bbb}: p<0.001 vs. Lean+saline

Table 5: Multiple regression analyses of the relation between mechanical properties (Stiffness), insulin resistance, cortical bone microarchitecture and bone compositional parameters.

Dependent variable	Groups	Model adjusted R^2	Model p value	Parameter	β	Parameter p value
Stiffness	Lean+saline vs HFD+saline	0.786	<0.001	Intercept	-104.873	0.023
				Mineral/matrix ratio	48.144	<0.001
				Tt.Ar	36.261	0.050
				HOMA-IR	-8.379	0.024
	HFD+saline vs HFD+sitagliptin	0.696	<0.001	Intercept	-65.014	0.029
				Mineral/matrix ratio	43.142	<0.001
				Collagen maturity	18.770	0.004
				HOMA-IR	-6.267	<0.001

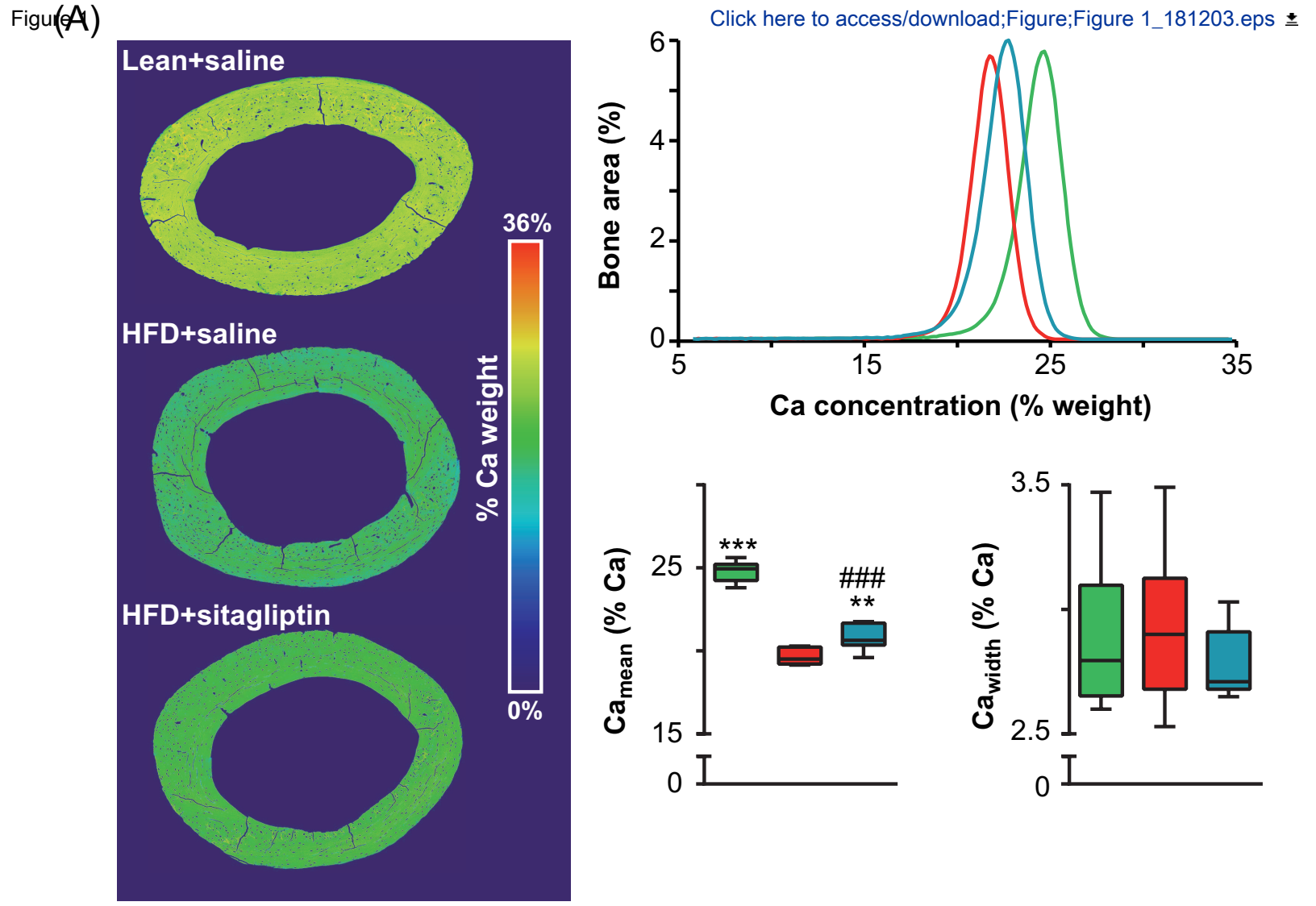

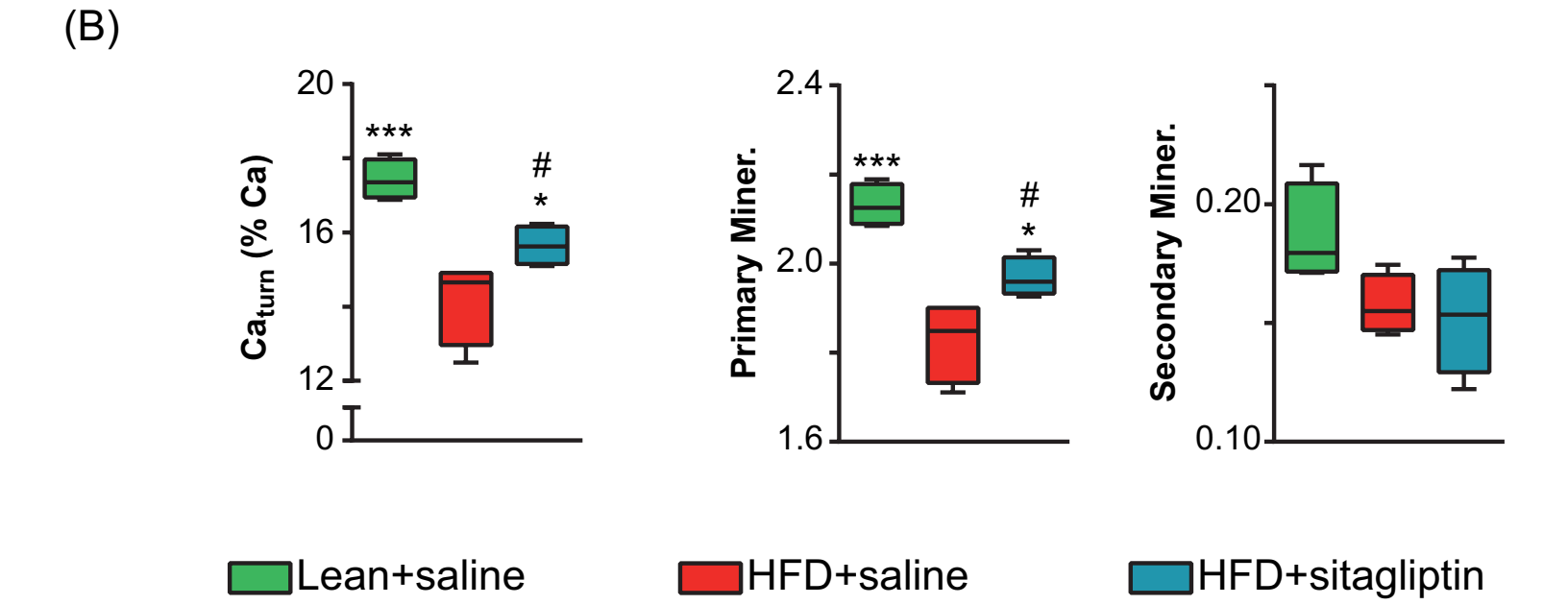

Figure 1

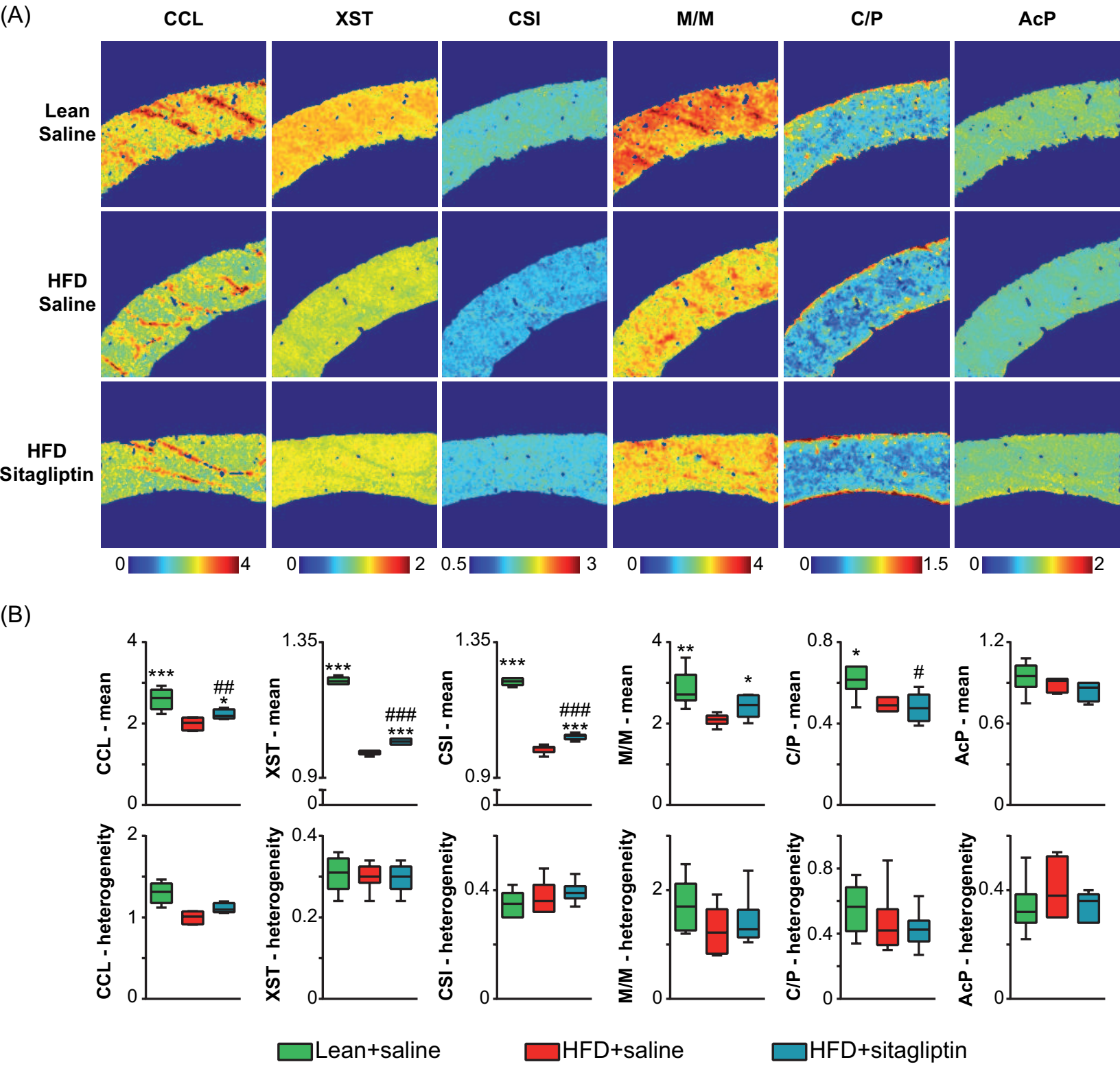

Figure 2